10.21611/qirt.2016.075

A round robin test of flash thermography – detectability and quantification of artificial and natural defects in CFRP and metal structures

by C. Maierhofer[1], N. Rothbart[2], M. Goldammer[3], F. Hohlstein[4], J. Koch[5], I. Kryukov[6], G. Mahler[7], B. Stotter[8], G. Walle[9], B. Oswald-Tranta[10], M. Sengebusch[11]

[1]Federal Institute for Materials Research and Testing (BAM), Unter den Eichen 87, 12205 Berlin, Germany, *christiane.maierhofer@bam.de*
[2]German Aerospace Center (DLR), Rutherfordstraße 2, 12489 Berlin, Germany, *nick.rothbart@dlr.de*
[3]Siemens AG Corporate Technology, Otto-Hahn-Ring 6, 81739 München, Germany, *matthias.goldammer@siemens.com*
[4]Block Materialprüfung GmbH, Johann-Hittorf-Straße 8, 12489 Berlin, Germany, *felix.hohlstein@mailbox.tu-berlin.de*
[5]edevis GmbH, Handwerkstr. 55, 70565 Stuttgart, Germany, *Joachim.Koch@edevis.de*
[6]University of Kassel, Kurt-Wolters-Str. 3, 34125 Kassel, Germany, *i.kryukov@uni-kassel.de*
[7]InfraTec GmbH Infrarotsensorik und Messtechnik, Gostritzer Str. 61-63, 01217 Dresden, Germany, *G.Mahler@infratec.de*
[8]University of Applied Science Upper Austria, Stelzhamerstraße 23, 4600 Wels, Austria, *bernhard.stotter@fh-wels.at*
[9]Fraunhofer Institute for Nondestructive Testing IZFP, Campus E3 1, 66123 Saarbrücken, Germany, *guenter.walle@izfp.fraunhofer.de*
[10]University of Leoben, Peter-Tunnerstrasse 27, 8700 Leoben, Austria, *beate.oswald@unileoben.ac.at*
[11]Deutsches Institut für Normung e. V., Am DIN-Platz, Burggrafenstraße 6, 10787 Berlin, Germany, *martin.sengebusch@din.de*

Abstract

Within the scope of a DIN INS project, a flash thermography round robin test that evaluates reliability, comparability, and efficiency of different testing situations was organized. The results give information about the detectability of defects, e.g. depending on their size and depth, the evaluation methods and the materials used. Besides, the influences of equipment and parameters used by the participants on the results were analysed. All of the quantitative results as well as the feedback given by the participants will be presented in a DIN committee in order to contribute to a flash thermography standard.

1. Introduction

With flash thermography a fast and sensitive non-destructive testing method for CFRP and metal structures is available that exhibits great potential for the integration into production processes. Typical applications for metal structures are the quality assurance of spot and laser welding joints [1], the detection of oblique cracks and overlaps and the control of soldered joints [2]. For testing of CFRP structures, flash thermography is well suited for proving adhesive bondings and for detecting and characterizing delaminations, impact damage, fibre deviations and inclusions of impurities [3, 4].

Despite the great potential of active thermography, there is still a lack of testing standards, reference test specimens, and round robin tests, which are required for harmonizing the testing procedure. The only known round robin tests for active thermography were conducted in 1998 and 2000 using CFRP specimens with impact damage [5, 6]. The aim of the trials of the former Eurotherm working group was the comparison of different excitation and evaluation techniques of active thermography by assessing the signal-to-noise ratio (SNR) of the detected flaws and further performance characteristics. Among other thermographic excitation methods, also flash thermography was evaluated. In 2007 an ASTM standard has been published titled ASTM E 2582-07 *Standard Practice for Infrared Flash Thermography of Composite Panels and Repair Patches Used in Aerospace Applications* [7]. Here, the testing procedures as well as the data analysis are described in detail, but quantitative information concerning the appropriate excitation energy and further measurement parameters is missing. Furthermore, the limitations of the method like penetration depth and detection sensitivity are not considered. Basic European standards on the application of thermography for NDT are currently under development [8, 9, 10]. For the development of a standard on flash thermography, systematic investigations on the influence of material, type of defects, measurement parameters, and data analysis were performed within a national funded standardization research project [11]. The main deliverables of that project are a draft document for a standard on flash thermography and several reference test specimens. For evaluating this draft standard, a new round robin test was carried out as a validation study in accordance with DIN EN ISO/IEC 17043:2010-05 [12]. In this study, a large variation of test equipment as well as of tested materials and structures was considered. Nine institutions from different backgrounds participated with different equipment. These institutions included universities, research

institutes, industrial companies and small and medium enterprises. 16 test specimens consisting of different metals (steel, aluminium and copper) and CFRP containing various artificial and natural defects were constructed. These test specimens represent different testing situations and enable qualitative and partially quantitative evaluation of the data. In the following, the conditions of the round robin test are described and selected results are presented. Here, these results are focused on test specimens made of different materials including flat bottom holes and of different CFRP test specimens with artificial delaminations and impact damage.

2. Description of the round robin test

2.1 Participants and equipment

The equipment and measurement parameters used by the nine participants of the round robin test for the large steel test specimen are listed in table 1. With the exception of one microbolometer infrared (IR) camera with 384 x 288 pixels, all IR cameras used contain indium antimonite (InSb) sensors with sizes of 320 x 256 to 640 x 512 pixels. All InSb cameras are sensitive in the mid wave infrared range (MWIR) varying from 1.5 - 5.1 µm (and thus including also parts of the NIR) to 3.5 - 5.7 µm. For the investigations at the metal test specimens, frame rates between 50 Hz (recommended frame rate) and 353 Hz were selected. For copper and aluminium, higher frequencies were used. The integration times were set between 720 and 2500 µs resulting in experimentally determined temperature resolutions (noise equivalent temperature difference NETD) at 30°C between 40 and 18 mK. The distances of the flash lamps to the sample and of the IR camera to the sample were between 24 and 80 cm and 33 and 81 cm, respectively. The angles of the flash lamps to the normal of the sample surfaces were set between 0 and 45°. For the IR camera, lenses with focal distances of 12 and 25 mm were used. These parameters resulted in spatial resolutions between 0.29 and 0.97 mm per pixel. With the exception of one participant, all used a temperature calibrated IR camera system.

Table 1. *Parameters of the experimental set-up used by each participant of the round robin test for the investigations at the steel test specimens.*

participant	A	B	C	D	E	F	G	H	I
flash									
energy in kJ	4 x 6	2 x 6.4	2 x 3	2 x 3	1 x 6	2 x 3	1 x 6	1 x 6	1 x 6
duration in ms	2.6	10	2	n. a.	11	2	10	8	1
distance in cm	30	25	30	24	36	50	35	35	80
angle in °	15	45	30	41	40	30	30	0	10
ΔT in K (see text)	7.2	8	11	4.2	n. a.	24	13.6	0.8	9
energy input in J/cm^2	1.7	1.9	2.6	1.0	n. a.	5.8	3.3	0.2	2.2
IR camera									
type of detector	InSb	InSb	InSb	micro-bolo-meter	InSb	InSb	InSb	InSb	InSb
wavelength in µm	2 - 5	2.5 - 5.1	3 - 5	7.5 - 14	1.5 - 5.4	3 - 5	3 - 5	3.5 - 5.7	1.5 - 5.1
array size in pixels	640 x 512	320 x 256	320 x 256	384 x 288	640 x 512	640 x 512	640 x 512	640 x 512	320 x 256
frame rate in Hz	50	50	300	50	353	100	50	200	50
integr. time in µs	720	800	1000	n. a.	2200	2500	2500	1560	1500
NETD in mK	< 25	30	< 20	< 40	18	20	< 20	45	< 20
distance in cm	65	70	70	49	64	48	67	33	81
IFOV in mrad	0.57	1.1	1.2	1.4	0.6	0.54	0.54	1.2	1.2
pixel size in mm	0.4	0.78	0.84	0.69	0.38	0.29	0.84	0.41	0.97

2.2 Test specimens

The test specimens described in the following sections were made of the following materials:

- Stainless steel (1.4301, X5CrNi18-10)
- Aluminium (3.3206, AlMgSi0.5)
- Copper (CW004A)
- CFRP with unidirectional and quasiisotropic orientation

The thermal parameters of these materials are listed in table 2. The thermal diffusivities were determined from transmission measurements as described in [4]. The mass density as well as the specific heat capacity were taken from

literature as indicated, while the thermal conductivity was calculated from these parameters using the relationship $\lambda = \alpha \rho c$.

Before the measurements were performed, all test specimens made of metal were blackened by all participants using the same graphite spray.

Table 2. *Thermal material parameters of the test specimens of the round robin test.*

Material	Diffusivity α in 10^{-5} m^2/s	Mass density ρ in kg/dm^3	Heat capacity c in J/(kg K)	Thermal conductivity λ in W/(m K)
Steel 1.4301 X5CrNi18-10	0.37 ± 0.02	7.9[a]	500[a]	14.6 ± 0.8
Aluminium 3.3206 AlMgSi0.5	5.0 ± 0.2	2.7[b]	900[c]	121 ± 5
Copper CW004A	9.8 ± 0.4	8.93[d]	386[d]	338 ± 14
CFRP with quasi-isotropic fibre alignment in the test specimen with FBH	0.025 ± 0.002[e]	1.5[f]	1200[g]	0.45 ± 0.04
CFRP with quasi-isotropic fibre alignment in the test specimen with stepped wedge and artificial delamination	0.022 ± 0.002[e]	1.5[f]	1200[g]	0.40 ± 0.04
CFRP with quasi-isotropic fibre alignment in the test specimen with impact damage	0.029 ± 0.002[e]	1.5[f]	1200[g]	0.52 ± 0.04
CFRP with quasi-isotropic fibre alignment in the test specimen with impact damage	0.026 ± 0.002[e]	1.5[f]	1200[g]	0.47 ± 0.04

[a] *www.thyssenkrupp.at*
[b] *www.retsch.dk*
[c] *http://www.aluminiumdesign.net/why-aluminium/material-comparison/*
[d] *www.kupferinstitut.de*
[e] *perpendicular to fibre orientation*
[f] *www.swiss-composite.ch*
[g] *www.aviogate.com*

2.2.1 Test specimens with flat bottom holes

Three large metal test specimens with a size of 200 x 200 x 7.5 mm^3 and three small metal test specimens with a size of 100 x 100 x 4.5 mm^3 made of stainless steel, aluminium, and copper and with flat bottom holes (FBH) of different sizes were constructed. For the large test specimens, the diameters of the holes were 8, 16 and 32 mm, and the remaining wall thicknesses (RWT) were varied between 2 and 6 mm, see figure 1.a. The small test specimens contained FBH with diameters of 1, 2 and 4 mm with RWT of 0.2 to 3.5 mm, see figure 1.b.

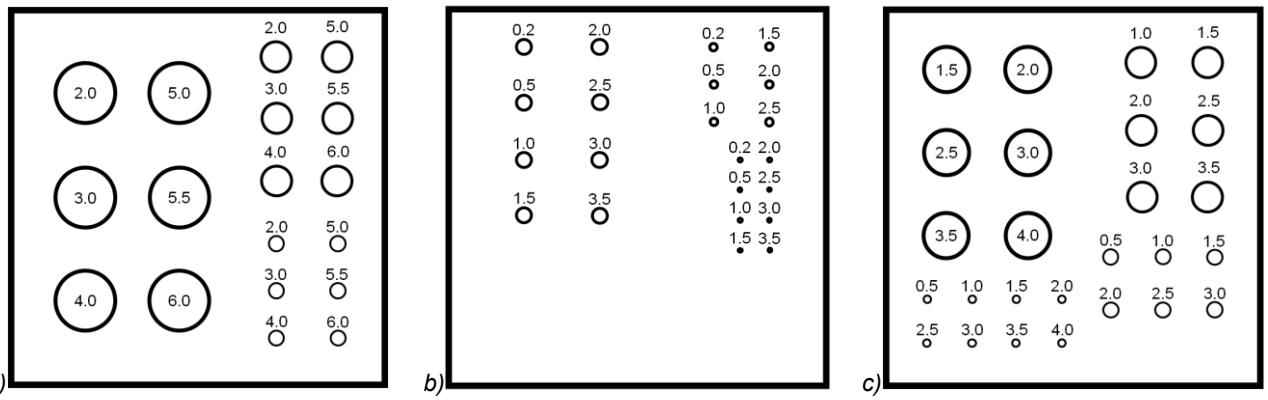

Fig. 1. *Sketches of a) large metal test specimens with sizes of 200 x 200 x 7.5 mm^3 and FBH with diameters of 8, 16, and 32 mm, b) small metal test specimens with sizes of 100 x 100 x 4.5 mm^3 and FBH with diameters of 1, 2, and 4 mm, c) CFRP test specimen with sizes of 200 x 200 x 6 mm^3 and FBH with diameters of 4, 8, 16, and 24 mm. The numbers are giving the RWT in mm.*

For CFRP, only one test specimen was assembled containing FBH with diameters of 4, 8, 16 and 24 mm and with RWT from 0.5 to 3.5 mm, see figure 1.c. It has to be considered that the geometry of this test specimen was different from the other large test specimens made of metal. The CFRP sheet consists of a quasiisotropic assembling of 32 layers of unidirectional carbon fabric $[0°/90°/+45°/-45°]_{8s}$, which were arranged mirror-symmetrical with respect to the middle plane. The fabric was put into the mould that was subsequently filled by epoxy according to the RTM (resin

transfer moulding) light method. The sheet was cured in the mould at 50 to 60°C for about 24 h. Afterwards, the FBH were milled into the plain sheet.

2.2.2 CFRP test specimens with artificial delaminations

The CFRP step wedge with artificial delaminations simulated by double layered polytetrafluoroethylene (PTFE) sheets has a size of 200 x 200 mm^2 with step widths of 40 mm and step heights of 1.5, 2.0, 2.5, 3.0, and 3.5 mm, see figure 2.a. The step wedge was assembled by CFRP pregregs (KUBD 1507) with unidirectional fibre orientation and a thickness of 0.14 mm each. The prepregs were oriented quasiisotropic [+45°/-45°/0°/90°] starting at +45°. First, seven prepregs were stacked up to a total thickness of 1 mm. Here, the first series of double layered PTFE sheets with sizes of 2 x 2, 3 x 3, 4 x 4, 8 x 8, and 16 x 16 mm^2 was positioned, see figure 2.b. Second, three prepreg layers were added and the next series was positioned, and so on. After finishing each step, the sizes of the prepregs were reduced by the width of one step. Therefore, the five different series of PTFE sheets have coverages of 0.5, 1.0, 1.5, 2.0 and 2.5 mm related to the top surface. The remaining wall thickness related to the bottom surface is the same for all series and is equal to 1 mm. The curing of the stepped wedge was performed at a pressure of 7.5 bar and a temperature of 120°C for about 120 min. Afterwards, the visual inspection by microscopy showed a regular layered structure with a very low porosity.

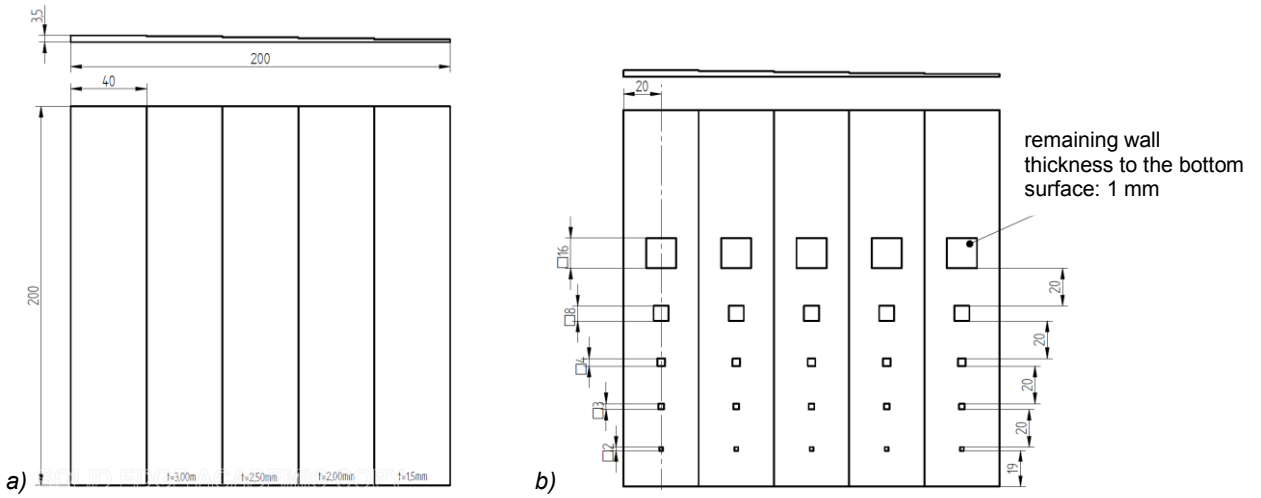

Fig. 2. *Sketches of the CFRP step wedge with artificial delaminations in different depths. a) Thickness of the different steps. b) Position and sizes of the artificial delaminations simulated by double layered PTFE sheets. All numbers are belonging to mm.*

2.2.3 CFRP test specimens with impact damage

For the test specimens with impact damage, three CFRP plates with quasiisotropic fibre orientation and three CFRP plates with a unidirectional one were manufactured. Each plate has a size of 150 x 100 x 3 mm^3 and consists of 18 layers of unidirectional carbon fabric. The same fabric was used as for the CFRP test specimen with FBH. For the quasiisotropic fibre orientation, these layers were oriented subsequently by 0°/+60°/-60°. For the unidirectional orientation, the fibres were oriented all parallel to the long side of the plate. The curing was performed as described in section 2.2.1.

Afterwards, defined impact damages were introduced with energies of 2.5, 5 and 10 J. These low velocity impacts were realized by a drop weight with two spherical impactors having a radius of 6 mm and masses of 0.627 kg and 1.285 kg. The different energies were realized by selecting the appropriate height of the impactor. Velocities between 2.8 and 4 m/s were reached.

2.3 Instructions for data recording and analysis

The inspection tasks of the round robin test contained measurements with flash thermography of all test specimens. While the test specimens with FBH had to be tested only in reflection configuration, it was preassigned to investigate the CFRP step wedge and the sheets with impact damage in reflection and transmission configuration. Different steps of the data analysis of selected thermograms and phase images were specified. The following specifications were given for the measurements at the above described test specimens:

- The experimental set-up consisting of one to four flash lamps, the IR camera and the test sample should be installed in such a way that an optimized energy input and a homogeneous illumination is provided. The minimum requirements were the use of at least one flash lamp with energy of at least 3 kJ and an IR camera with a frame rate of at least 50 Hz, an NETD of less than 60 mK and the ability to record

sequences. It was recommended to use polymethylmethacrylate (PMMA) plates or glass plates in front of the flash lamps to reduce the direct infrared radiation from the lamps after heating up due to the flash.

- The homogeneity of the illumination should be verified by using a thin metal sheet and the input energy density should be determined by measuring the temperature rise of a supplied sensor plate in the plane of the test specimen. This sensor plate consisted of a silver plate with a size of 10 x 10 x 1 mm^3 [13].
- Frames should be recorded before, during and after flash excitation, until no contrast could be detected any more. Measurement duration of 30 s was recommended at least for the steel and CFRP test specimens.
- For data analysis, the following topics were specified:
    - Documentation of the temperature rise of the silver plate.
    - Subtraction of one of the thermograms recorded before the flash from the whole thermal sequence.
    - Selection of thermograms at distinct times from the recorded cooling down sequences providing an optimum temperature contrast of the defects. For different defects, thermograms at different times t_s might be selected.
    - Application of pulse phase thermography (PPT) to the data recorded after the flash and selection of phase images providing an optimum phase contrast of the defects at those frequencies. For different defects, phase images at different frequencies f_s might be selected.
    - Documentation of the detectability of all visible defects in the thermograms and phase images.
    - Measurement and documentation of the size of the impact damage in the CFRP plates with quasiisotropic and unidirectional fibre orientation.

3. Results

3.1 Detectablity of flat bottom holes in metal and CFRP test specimens

The detectability of the FBH in each test specimen described in chapter 2.2.1 is displayed in figure 3. Detectability means that the defect could be detected at least in one of the thermograms or in one of the phase images. Here it is shown how often each hole could be detected by the nine participants. In the steel test specimen (figure 3.a) the holes with a diameter of 32 mm and RWT from 2 to 4 mm could be detected by all participants, while the hole with a diameter of 8 mm and a RWT of 6 mm could be detected only by three participants. The smaller number of detections of deeper holes can be explained by the limited penetration depth within the model of thermal waves. Holes with smaller diameters are detected less often (for similar RWT), as the contrast is reduced by lateral heat diffusion processes. For the larger aluminium test specimen (see figure 3.c), the data are more or less similar to the steel test specimen. For the larger copper test specimen (see figure 3.e), all deeper FBH could be detected less often than for the other materials. For the small test specimens, there is a larger difference between the detectability of the FBH in steel and in aluminium, where less FBH could be detected in aluminium. In CFRP, a bit less FBH with a diameter of 8 mm and similar RWT could be detected than in copper.

The number of all detected FBH in each test specimen (and thus for each material) and for each participant is visualized in the diagrams in figure 4. First of all, from these diagrams it is obvious that the number of detected holes is very low for participant D, who used the microbolometer IR camera. For the other participants, the number of detected holes in steel and CFRP is similar, while the participants are divided into two groups concerning the detection of FBH in copper. While this number was higher for participants A, B, C and E, it was lower for participants F, G, H and I. Partly, this could be explained by the used frame rates as well as by the procedures, which were used for calculating the phase images.

3.2 Detectablity of artificial delaminations in a CFRP stepped wedge test specimens

Figure 5 shows the results of the investigations of the CFRP step wedge test specimen with artificial delaminations. This test specimen was investigated by eight participants in reflection and transmission configuration. The detectability of the defects was analyzed in the thermograms as well as in the phase images. For both configurations, the phase images show more defects than the thermograms. These phase images, optimized for each step, are displayed in figure 5.e and 5.f as a result of one of the participants. The total numbers of detections for each defect and for all participants except participant D are shown in figure 5.a to 5.c, thus each defect could be detected with a maximum number of eight. Here, it is evident that much more defects could be detected in transmission configuration than in reflection configuration (see figure 5.d as well). It has to be considered that in the diagrams in 5.a to c, the thickness of the single steps is displayed on the x-axes. The coverage of each delamination to the top surface is 1 mm less than the thickness. By comparing the detectability of similar sizes and RWT of the delaminations to that of the FBH (i. e. figure 5.b and figure 3.g, the detectability of the FBH is considerably higher.

10.21611/qirt.2016.075

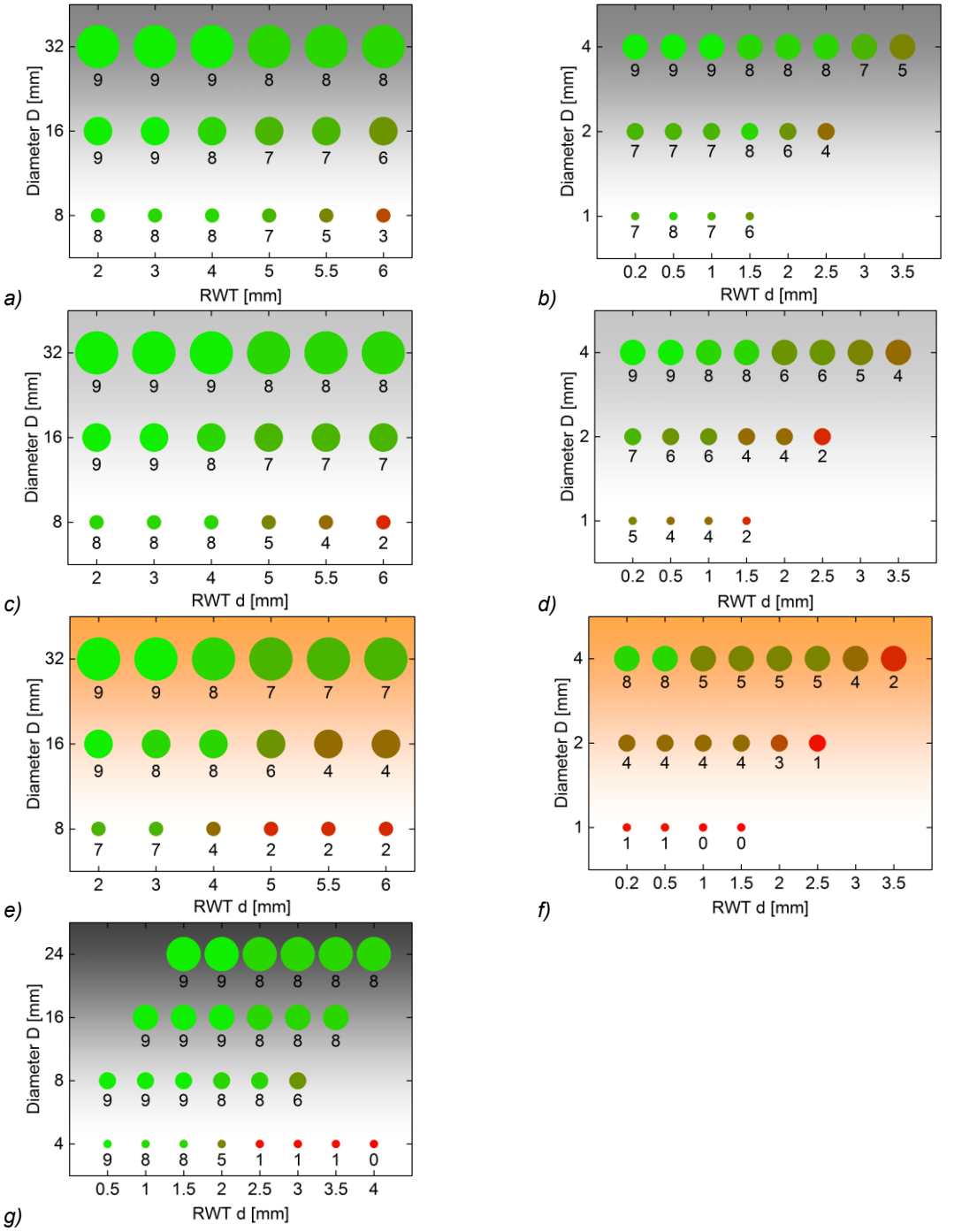

Fig. 3. *Detectability of flat bottom holes in a, b) steel, c, d) aluminium, e, f) copper and g) CFRP as a function of hole diameter D and remaining wall thickness d for all nine participants. Thus the maximum number of detections for each FBH was nine.*

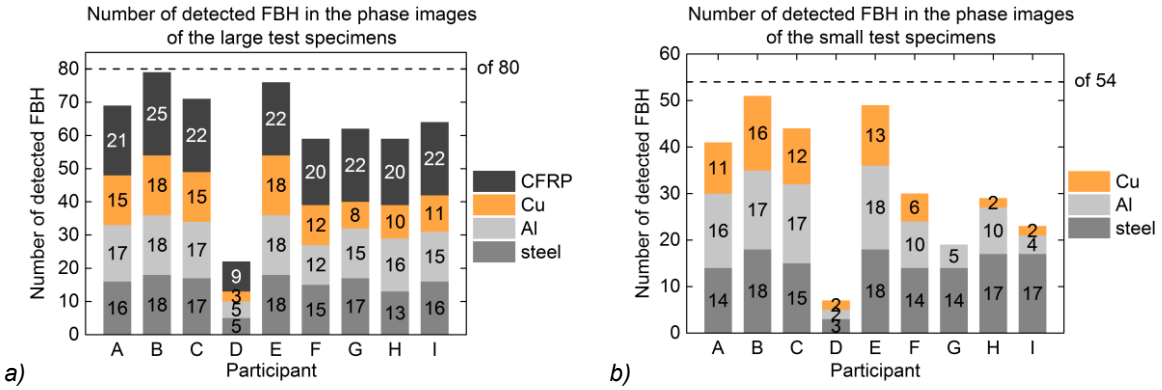

Fig. 4. *Number of detected flat bottom holes for each participant and each material in a) the large test specimens and b) the small test specimens.*

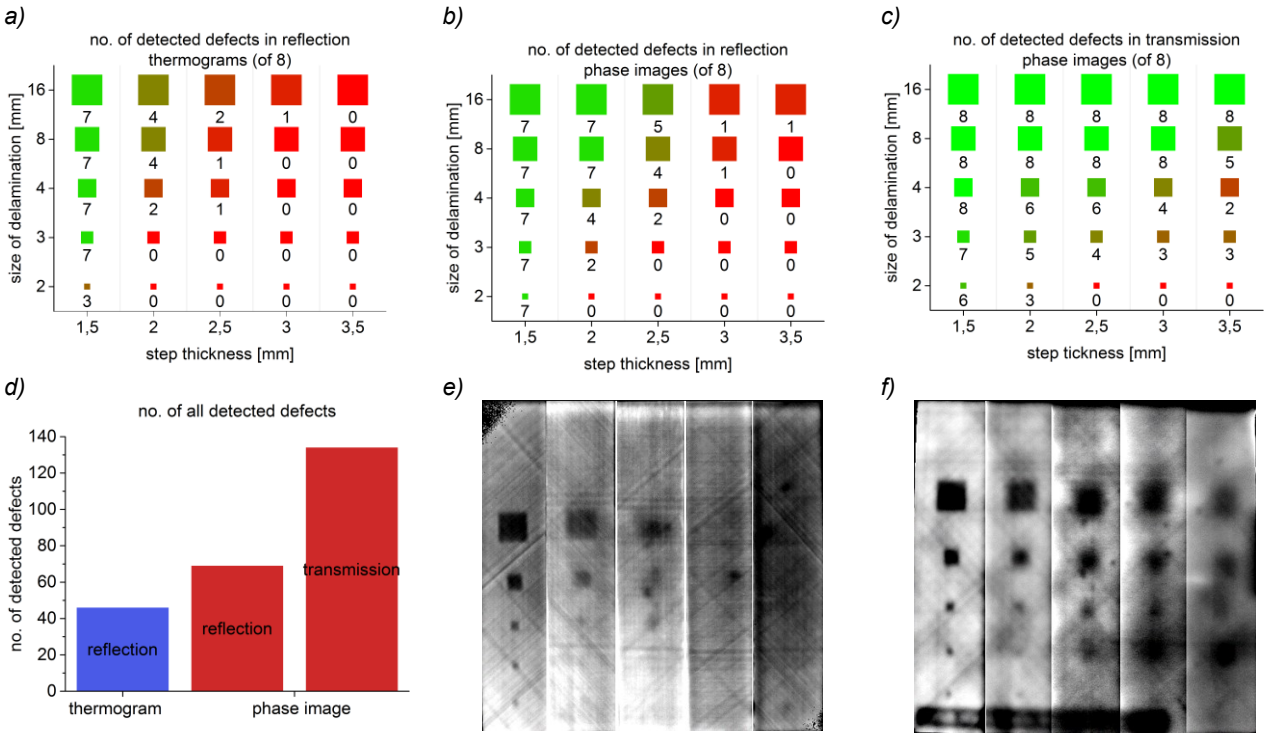

Fig. 5. *Results of flash thermography testing at the CFRP step wedge test specimen with artificial delaminations (PTFE plates) with different sizes at various depths. a to c) Number of detected defects of eight participants obtained from the thermograms and phase images in reflection configuration and from the phase images in transmission configuration. d) Comparison of the number of detected defects by all participants depending on the measurement configuration and on the method of data analysis. e) Phase images (optimized for each step) from a sequence recorded in reflection configuration. f) Phase images (optimized for each step) from a sequence recorded in transmission configuration.*

3.3 Determination of the size of impact damages in unidirectional and quasiisotropic CFRP sheets

Figure 6 shows the photos in the visible spectrum of the different impact damages at the quasiisotropic (qi) and unidirectional (ud) CFRP test specimens that were taken at the front and the back sides of the sheets. Already at the front surface, a clear indent of the impactor is visible for all impact energies. Size and shape of the indent are similar for the qi and ud material. The diameter of the indent is increasing with the impact energy. At the back side, for all impacts a clear buckling of the material is visible. For the two higher energies, cracks are detectible. At the back side of the ud samples, the impact damages have an elliptic shape where the longer axis is oriented parallel to the fibres.

In figure 7, the phase images and thermograms of one of the participants (C) are displayed. Here, the phase images recorded in reflection configuration and the thermograms from the transmission configuration were selected. In both types of images, the defects have similar sizes. It can be observed that with increasing impact energy, the size of the defects is increasing. Again, the elliptic shape of the defects in the ud samples can be recognized.

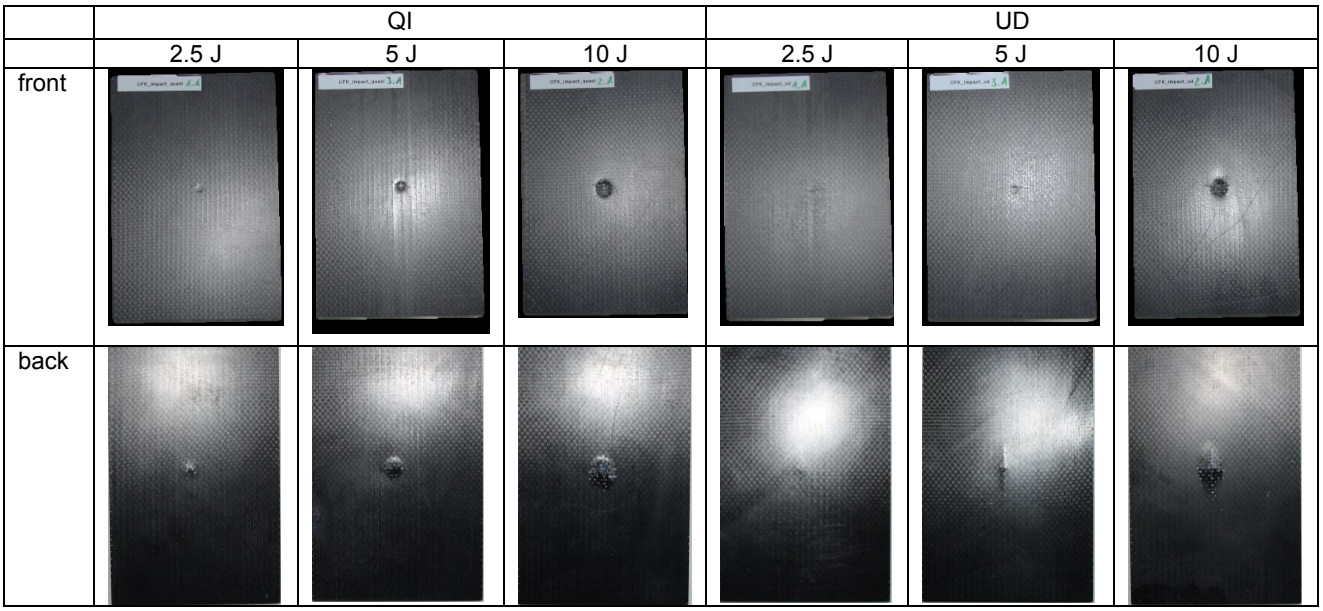

Fig. 6. *Photos of the CFRP test specimens with impact damages of 2.5, 5 and 10 J. The three columns on the left show the photos of the quasiisotropic sheets and the three columns on the right those of the unidirectional sheets. The photos of the front side are displayed in the first row, those of the back side in the second row.*

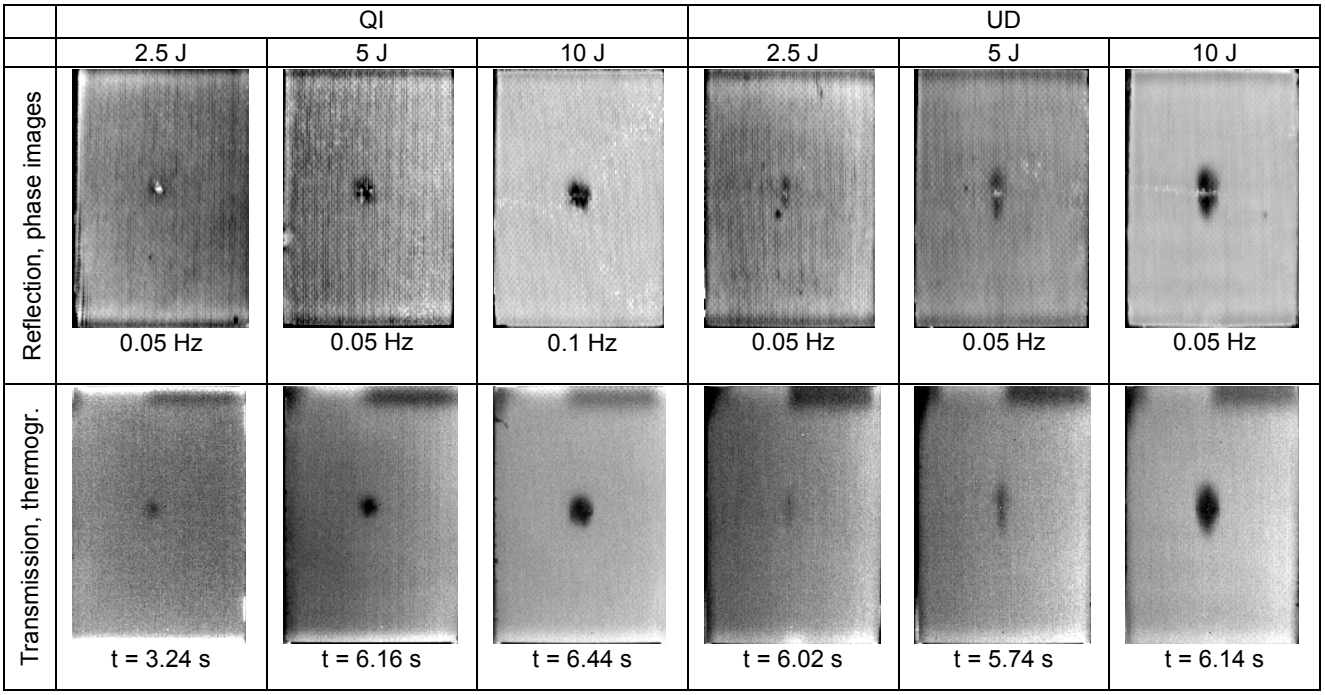

Fig. 7. *Phase images and thermograms of the CFRP test specimens with impact damages of 2.5, 5 and 10 J of one participant (C). The three columns on the left show the results of the quasiisotropic sheets and the three columns on the right those of the unidirectional sheets. The phase images of the reflection configuration are displayed in the first row, the thermograms of the transmission configuration in the second row.*

Figure 8.a shows the mean values of the horizontal and vertical sizes of the defects of all participants that were measured in the phase images recorded in reflection configuration. The left diagram shows the data of the qi sheets, the right one those of the ud sheets. Furthermore, the data of the different impact energies are separated by different grey values. From these diagrams, it can be observed that the defect sizes are increasing with the impact energy and that the defect sizes in the ud sheets are significantly larger than in the qi sheets. For the ud sheet, the horizontal extension of

the defect is significantly larger than the defect size in vertical direction. But for the qi sheet as well, the horizontal size is slightly larger than the vertical size. This might be explained by the geometry of the sheets and how these were fixed in the sample holder of the falling weight system.

The data of each participant of the sizes of the 5 J impact damage in the qi sheet and the ud sheet are displayed in the two diagrams in figure 8.b. For the defect in the qi sheet, the deviations are up to 5 mm in horizontal as well as in vertical direction. But for the defect in the ud sheet, much larger deviations up to 10 mm are observed. For a better visualization of these deviations, figure 9 shows the selected phase images of the 5 J samples of all participants. From these phase images, it becomes clear that the sizes of the damages in the images depend on the selected frequency. E. g. participant F could hardly detect the defect in the ud sheet. Here, probably the selected frequency of 0.25 Hz was close to the blind frequency. But the measured defect sizes might also depend on how the participants have performed the geometrical measurements. E. g. although the phase images of participant B and participant C were recorded at similar frequencies and although the defects are appearing very similar in the images, the horizontal and vertical values showed deviations of up to 3 mm in both sheets.

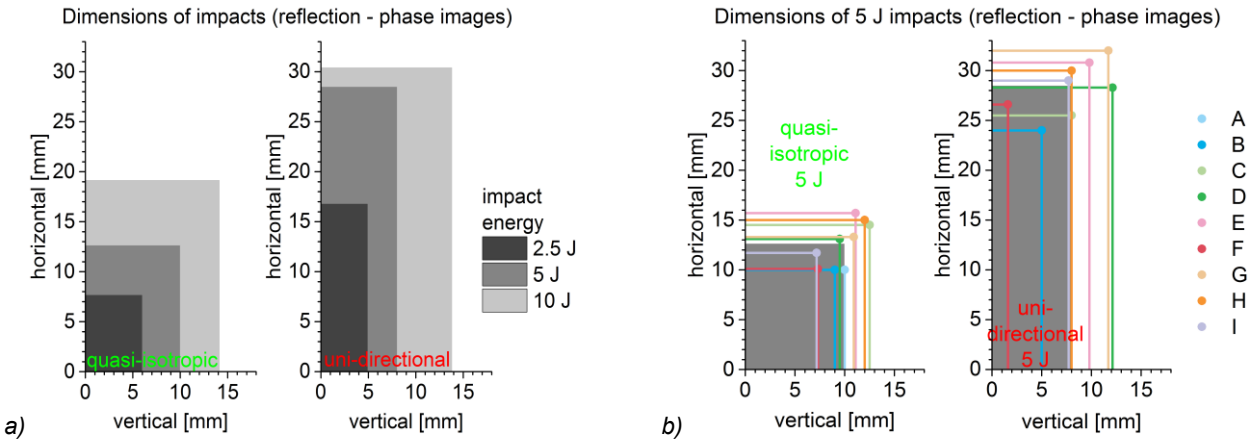

Fig. 8. *Sizes of the impact damages measured in the phase images recorded in reflection configuration. a) Mean values of all participants for all defects. b) Mean (grey shading) and individual values of all participants for the 5 J impact damage. The vertical direction was parallel to the short side of the sheet, the horizontal direction parallel to the long side.*

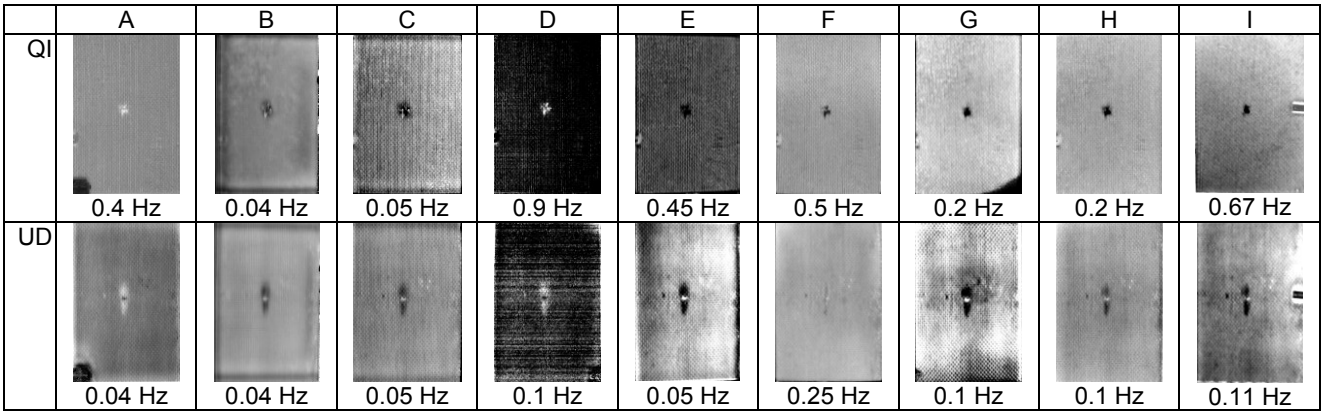

Fig. 9. *Phase images of all participants recorded at the 5 J impacts of the qi sheets (top row) and of the ud sheets (bottom row).*

4. Conclusions

At the round robin test of flash thermography, nine institutions participated with different equipment. Most of the participants used an IR camera with an InSb detector and with detector sizes of 320 x 256 or 640 x 512 pixels. Different amounts of excitation energies of the flash were introduced into the test specimens. In this contribution, the detectability of FBH in different materials (steel, aluminium, copper and CFRP), the detectability of artificial delaminations in CFRP and the sizes of impact damages in quasiisotropic and unidirectional CFRP are compared. This comparison shows a large scattering of the results concerning particularly:

- the detectability of FBH with smaller diameters and larger RWT in aluminium and copper
- the detectability of artificial delaminations with smaller sizes and larger coverages in the phase images recorded in transmission configuration
- the sizes of the impact damages in unidirectional sheets in the phase images recorded in reflection configuration

This scattering can be explained by:

- different amounts of flash energy introduced into the specimens
- different measurement parameters (frame rate, integration time, NETD, spatial resolution)
- different methods for data analysis (parameters of PPT, selection of appropriate thermograms and phase images for each defect)
- large inaccuracy of geometrical measurements of defect sizes within the thermograms or phase images

None of the topics could be related to the scattering of the results alone.

The results of this round robin test will be used to complement the draft standard of flash thermography. In detail, this will concern the appropriate selection of flash lamps, IR camera and measurement parameters, the verification of the experimental set-up and measurement parameters using reference test specimens, the appropriate selection of parameters for data analysis (e. g. start frame und number of frames for PPT), and examples and templates for test instructions and test protocols.

ACKNOWLEDGEMENTS

The project was funded within the program Innovations with Norms and Standards (INS 1255) by the German Federal Ministry of Economics and Energy. Within DIN e. V., the Standards Committee Materials Testing (NMP) was responsible for the project. The CFRP test specimens were constructed by *Zentrum für Faserverbunde und Leichtbau Haldensleben*.

REFERENCES

[1] Jonietz F., Ziegler M., Myrach P., Suwala H., Rethmeier M., "Untersuchung von Punktschweißverbindungen mit aktiver Thermografie", in: Proceedings of DACH-Tagung 2015, Salzburg, Österreich, 2015, http://www.ndt.net/article/dgzfp2015/papers/mi3c4.pdf

[2] Maierhofer C., Röllig M., Steinfurth H., Ziegler M., Kreutzbruck M., Scheuerlein C., Heck S., Non-destructive testing of Cu solder connections using active thermography, NDT & E International - Vol. 52, pp. 103-111, 2012.

[3] Maierhofer C., Röllig M., Ehrig K., Meinel D., Céspedes-Gonzales G., Validation of flash thermography using computed tomography for characterizing inhomogeneities and defects in CFRP structures, Composites Part B: Engineering - Vol. 64, pp. 175-186, 2014.

[4] Maierhofer C., Myrach P., Reischel M., Steinfurth H., Röllig M., Kunert M., Characterizing damage in CFRP structures using flash thermography in reflection and transmission configurations, Composites Part B: Engineering - Vol. 57, pp. 35-46, 2014.

[5] Vavilov V. P., Almond D. P., Busse G., Grinzato E., Krapez J.-C., Maldague X., Marinetti S., Peng W., Shirayev V., Wu D., "Infrared thermographic detection and characterization of impact damage in carbon fibre composites: results of the round robin tests", in: Proceedings of QIRT Conference 1998, Lodz, Poland, 1998, http://qirt.gel.ulaval.ca/archives/qirt1998/papers/005.pdf

[6] Almond D. P., Ball, R. J., Dillenz, A., Busse, G., Krapez, J.-C., Galmiche, F., Maldague X., "Round Robin comparison II of the capabilities of various thermographic techniques in the detection of defects in carbon fibre composites", in: Proceedings of QIRT Conference, Reims, France, 2000, http://qirt.gel.ulaval.ca/archives/qirt2000/papers/065.pdf

[7] ASTM E2582 - 07 (2014) Standard Practice for Infrared Flash Thermography of Composite Panels and Repair Patches Used in Aerospace Applications, ASTM International, West Conshohocken, PA, 2014

[8] prEN 16714-1:2014; Non-Destructive Testing—Thermographic Testing—Part 1: General Principles; , Beuth Verlag, Berlin, Germany, 2014

[9] prEN 16714-2:2014; Non-Destructive Testing—Thermographic Testing—Part 2: Equipment; , Beuth Verlag, Berlin, Germany, 2014

[10] prEN 16714-3:2014; Non-Destructive Testing—Thermographic Testing—Part 3: Terms and definitions, Beuth Verlag, Berlin, Germany, 2014

[11] Maierhofer C., "Entwicklung von Normen und Standards für die aktive Thermografie mit Blitzlichtanregung; Abschlussbericht zum Vorhaben", Technische Informationsbibliothek u. Universitätsbibliothek, Hannover, Germany, 2013, 45 pages, https://www.tib.eu/de/suchen/download/?tx_tibsearch_search%5Bdocid%5D=TIBKAT%3A815242689&cHash=fb8394d435add5d233e8f35a45527863#download-mark

[12] DIN EN ISO/IEC 17043:2010-05 Conformity assessment - General requirements for proficiency testing, Beuth Verlag, Berlin, Germany, 2010

[13] Krankenhagen R., Maierhofer C., Measurement of the radiative energy output of flash lamps by means of thermal thin probes, Infrared Physics & Technology - Vol. 67, pp. 363-370, 2014.